Robotica (2016) volume 34, pp. 2056–2070. © Cambridge University Press 2015
doi:10.1017/S0263574714002732

On the kinematics of a new parallel mechanism with Schoenflies motion

Po-Chih Lee and Jyh-Jone Lee*

Department of Mechanical Engineering, National Taiwan University, No. 1, Section 4, Roosevelt Road, Taipei 10617, Taiwan ROC.

(Accepted November 11, 2014. First published online: January 13, 2015)

SUMMARY

This paper investigates the kinematics of one new isoconstrained parallel manipulator with Schoenflies motion. This new manipulator has four degrees of freedom and two identical limbs, each having the topology of Cylindrical–Revolute–Prismatic–Helical (C–R–P–H). The kinematic equations are derived in closed-form using matrix algebra. The Jacobian matrix is then established and the singularities of the robot are investigated. The reachable workspaces and condition number of the manipulator are further studied. From the kinematic analysis, it can be shown that the manipulator is simple not only for its construction but also for its control. It is hoped that the results of the evaluation of the two-limb parallel mechanism can be useful for possible applications in industry where a pick-and-place motion is required.

KEYWORDS: Isoconstrained; Parallel manipulator; Schoenflies motion; Singularity; Condition number.

Nomenclature

$\boldsymbol{A}_{ij}$:	4×4 matrix of transformation between the jth and $(j+1)$th local frames of the ith limb.
C :	cylindrical pair.
d_{ij} :	translational distance between the jth and $(j+1)$th local frames of the ith limb.
$\boldsymbol{E}_i$:	4×4 matrix of ending matrix of the ith limb.
F :	degrees of freedom of a mechanism or mechanical manipulator.
f :	distance between the origin of the coordinate system on end-effector and coordinate system 4.
H :	helical joint.
$\boldsymbol{J}$:	Jacobian matrix.
$\boldsymbol{J}_{\mathrm{x}}$:	forward Jacobian matrix.
$\boldsymbol{J}_{\mathrm{q}}$:	inverse Jacobian matrix.
L :	distance between two cylindrical pairs along Z_0 axis
P :	prismatic joint.
p_i :	reduced pitch of the ith limb.
R :	revolute joint.
$\boldsymbol{S}_i$:	4×4 matrix of initial matrix of the ith limb.
${}^0\boldsymbol{T}_i$:	posture matrix of the end-effector for the ith limb.
$X_{\mathrm{E}}, Y_{\mathrm{E}}, Z_{\mathrm{E}}$:	position of the end-effector.
θ_{ij} :	joint angle between two adjacent normals of jth and $(j+1)$th local frames on the ith limb.
ϕ :	rotation of the end-effector.
$\kappa(\boldsymbol{J})$:	condition number of matrix J.

* Corresponding author. E-mail: jjlee@ntu.edu.tw

1. Introduction

For decades, a large amount of research has been devoted to six-degree-of-freedom (DoF) parallel manipulators. This type of manipulator, such as the Stewart–Gough platform,[1] may perform sophisticated work where a six-DoF motion is required. However, it is not conveniently used in industry because of its complex structure and being complicated to control. In addition, sophisticated manipulators are not commonly applied in manufacturing operations because those manipulators with higher mobility are not always needed in practical operations, and may suffer from a small workspace restricted by singularities. For these reasons, some applications in industry use parallel manipulators with lower mobility to perform tasks that do not require the six-DoF motion. For example, to move a product in a simple pick-and-place motion may require a three-DoF manipulator with translational motion. Alternatively, in many occasions where three translational and one rotational motions are required, a manipulator with Schoenflies motion may suffice. Plenty of existing robots can generate Schoenflies motion (also called *X*- or *SCARA*-motion), which consists of independent spatial translational motions and one rotational motion.[2–15] Clavel paved a new way to research on parallel manipulators by focusing on lower mobility and proposed the Delta architecture.[2,3] Angeles *et al*.[4,5] proposed a new overconstrained structure with Schoenflies motion. Pierrot provided a parallel mechanism, H4,[6] based on the same technology as the Delta robot. The idea of the articulated traveling plate was investigated and new prototypes with four DoF to achieve the Schoenflies motion were presented.[7,8] Dual-4[9] is a concept of a parallel manipulator standing on the Archi architecture[10] which is originally a three-DoF planar robot. Richard *et al*.[11] and Kong and Gosselin[12] introduced a partially decoupled four-DoF parallel mechanism producing the Schoenflies motion, the Quadrupteron robot, which contains revolute, prismatic, and cylindrical joints. The commercialized "Quattro" manipulator,[13] an industrial device with the fastest operations, was already developed by ADEPT Technology. These types of manipulators are widely utilized in industry.[14]

A few types of two-limbed isoconstrained parallel manipulators that can generate Schoenflies motion were synthesized by Lee and Hervé.[15] In the paper, a method for generating isoconstrained parallel manipulators with Schoenflies motion was proposed and a few general configurations were enumerated. However, the paper did not consider many details about the possible application and kinematics of any of the synthesized manipulators. More configurations relevant to possible applications were derived from the general type and discussed in refs. [16]–[18]. Compared with the existing 3T1R parallel robots, the two-limbed architecture of these isoconstrained parallel manipulators is more compact in volume and easier to control. Moreover, the non-overconstrained structure is less sensitive to manufacture errors. In fact, this type of manipulator shows a new concept of maneuvering the orientation of the end-effector by coaxial helical pairs with distinct pitches. This results in a more compact size of the manipulator than the existing Schoenflies-motion robots, such as the Delta robot which needs a fourth limb to perform the rotations of the end-effector. In this work, one of the enumerated configurations with limbs of the form, C–R–P–H joints, is investigated for its kinematic characteristics to evaluate its potential application. The remainder of the paper is organized as follows. The architecture of the manipulator is briefly introduced. Then, the forward and inverse kinematics of the manipulator are derived. Subsequently, the Jacobian and inverse singular configurations of the manipulator are also investigated. The workspace of the manipulator is discussed in Section 5. In Section 6, a performance index is applied to help characterize the properties of the manipulator. Finally, a conclusion of the manipulator characteristics is presented.

2. Descriptions of the Mechanism

2.1. Architecture of the robot

Figure 1 shows the schematic diagram of the manipulator where the fixed base is labeled as link 1 and the end-effector is labeled as link 5. Two identical limbs connect the end-effector to the fixed base. Each limb consists of three links. The three links in each limb and the end-effector are connected by the cylindrical (C), revolute (R), prismatic (P), and helical (H) joints from proximal to distal from the base. The joint axes of the two cylindrical pairs are not necessarily orthogonal; yet they are arranged to be orthogonal to each other for the sake of clarity.

This new structure is derived from the general type isoconstrained parallel manipulator with Schoenflies motion–$\underline{\mathrm{P(HH)}}_{\mathrm{u}}\mathrm{PH}_{\mathrm{w}}$-//- $\underline{\mathrm{P(HH)}}_{\mathrm{v}}\mathrm{PH}_{\mathrm{w}}$[15] The subscripts u, v, and w denote the orientations

https://doi.org/10.1017/S0263574714002732 Published online by Cambridge University Press

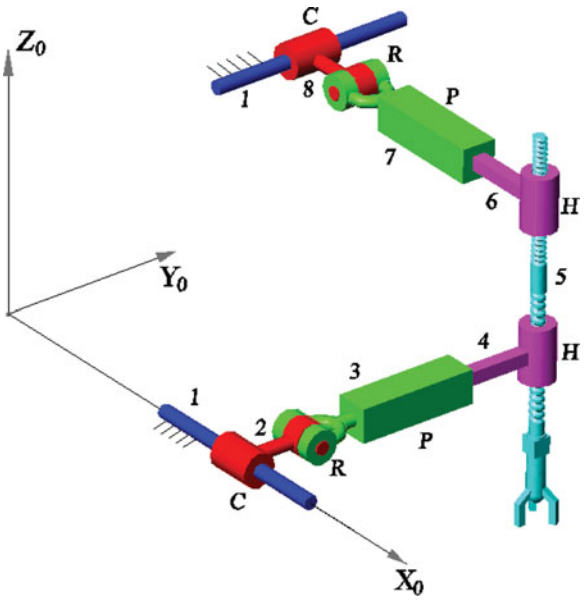

Fig. 1. Isoconstrained parallel manipulator with X- motion–$C_uR_uPH_w$-//-$C_vR_vPH_w$.

of the joint axes which are parallel to the X_0, Y_0, and Z_0 axes respectively and the underscore "_" denotes the axes of the marked joints are coaxial. If the pitches of the helical pairs in $(HH)_u$ and $(HH)_v$ are set to zero, a new architecture, $\underline{P(RR)}_u\underline{PH}_w$-//-$\underline{P(RR)}_v\underline{PH}_w$, can be generated in which the subscript represents the direction of the joint axis. Furthermore, if the first and second joints, P and R, are combined and replaced by the cylindrical pair C adjacent to the base, this results in the final structure, $C_uR_uPH_w$-//-$C_vR_vPH_w$ (abbreviated to CRPH). Overall, there are eight links and joints in the manipulator. The general Grübler–Kutzbach DoF equation well predicts that the DoF of the manipulator is $F = \lambda(n - 1) - 4J_2 - 5J_1 = 6(8–1)–4 \times 2–5 \times 6 = 4$. Therefore, the mechanism is isoconstrained (non-overconstrained) and the mobility is less sensitive to geometry errors compared to the overconstrained type of Schoenflies-motion robots.

In the CRPH manipulator, the C–R joints are easier to build than H–H joints in the primitive structure.[15] From a practical point of view, an actuating two-DoF cylindrical joint can be achieved by the revolute–helical (RH) chain or the revolute–prismatic (RP) chain, or the R–H–P–R chain where all joints are coaxial with the R joints. For the last case, the actuation of each leg can be realized by installing the rotary actuators at the R joints on the R–H–P–R chain. In addition, the rotation of the end-effector is caused by differential movements of the two coaxial H pairs with distinct pitches and is controlled by the angular displacements of the two cylindrical joints. This robot has a simple structure with two identical limbs, each limb providing two active motions. Further, one of the actuated motions directly reflects to X (or Y) motion of the end-effector and makes the robot easy to control in X–Y motion. In what follows, we will investigate the kinematics of this robot and show that it has simple analytical closed-form solutions.

2.2. Verification of four-DoF Schoenflies motion

To investigate the kinematics of the CRPH manipulator, the Denavit–Hartenberg method[19,20] is adopted in this work. As shown in Fig. 2, a fixed reference coordinate system is defined as $X_0 - Y_0 - Z_0$. The local coordinate system on each link is also depicted in the figure. For the coordinate systems chosen, the D-H parameters between two coordinate systems are given in Table I, where a_{ij} is the offset distance between two adjacent joint axes, α_{ij} is the twist angle between two z-axes, d_{ij} is the translational distance between two x-axes and θ_{ij} is the joint angle between two adjacent normals of a joint axis. In each parameter, the first subscript i indicates the number of limb, while the second subscript j indicates the number of the local coordinate system on the joint. Then, the coordinate transformation matrix between two adjacent coordinate systems, jth and $(j+1)$th, in the first limb can be respectively written as

https://doi.org/10.1017/S0263574714002732 Published online by Cambridge University Press

Table I. Link parameters and variables of the CRPH manipulator.

	First limb				Second limb			
j	a_{ij}	α_{ij}	d_{ij}	θ_{ij}	a_{ij}	α_{ij}	d_{ij}	θ_{ij}
1	a_{11}	0	d_{11}	θ_{11}	a_{21}	0	d_{21}	θ_{21}
2	0	$\pi/2$	0	θ_{12}	0	$\pi/2$	0	θ_{22}
3	0	$\pi/2$	d_{13}	$\pi/2$	0	$\pi/2$	d_{23}	$3\pi/2$
4	0	π	$-d_{14}$	θ_{14}	0	π	$-d_{24}$	θ_{24}

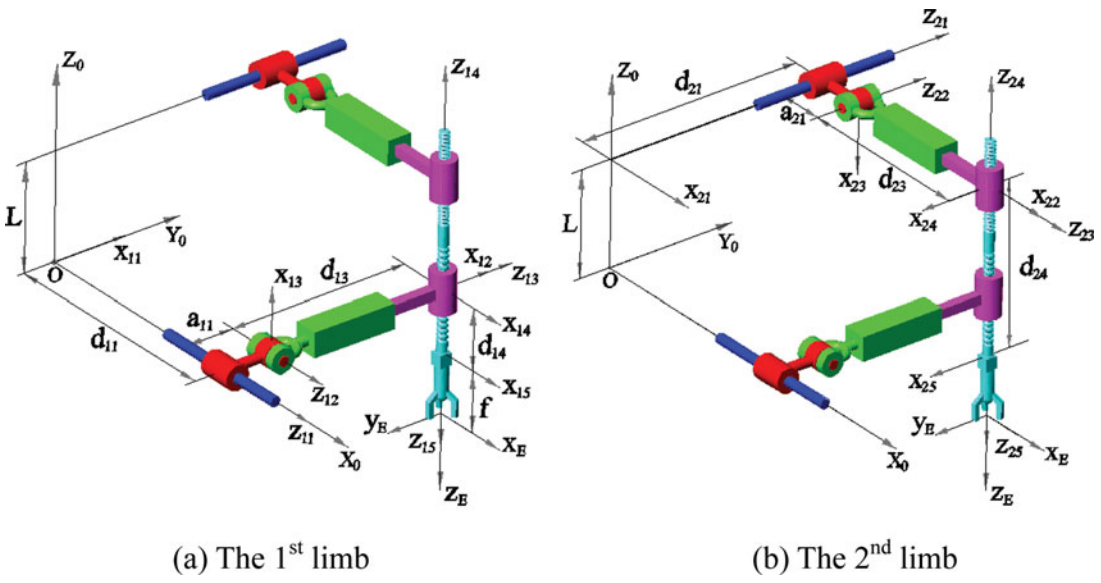

(a) The 1st limb (b) The 2nd limb

Fig. 2. Coordinate systems and parameters of CRPH manipulator. (a) The 1^{st} limb. (b) The 2^{nd} limb.

$$A_{11} = \begin{bmatrix} \cos\theta_{11} & -\sin\theta_{11} & 0 & a_{11}\cos\theta_{11} \\ \sin\theta_{11} & \cos\theta_{11} & 0 & a_{11}\sin\theta_{11} \\ 0 & 0 & 1 & d_{11} \\ 0 & 0 & 0 & 1 \end{bmatrix}, \quad A_{12} = \begin{bmatrix} \cos\theta_{12} & 0 & \sin\theta_{12} & 0 \\ \sin\theta_{12} & 0 & -\cos\theta_{12} & 0 \\ 0 & 1 & 0 & 0 \\ 0 & 0 & 0 & 1 \end{bmatrix},$$

$$A_{13} = \begin{bmatrix} 0 & 0 & 1 & 0 \\ 1 & 0 & 0 & 0 \\ 0 & 1 & 0 & d_{13} \\ 0 & 0 & 0 & 1 \end{bmatrix}, \quad A_{14} = \begin{bmatrix} \cos\theta_{14} & \sin\theta_{14} & 0 & 0 \\ \sin\theta_{14} & -\cos\theta_{14} & 0 & 0 \\ 0 & 0 & -1 & -d_{14} \\ 0 & 0 & 0 & 1 \end{bmatrix}. \tag{1}$$

Note that the first local coordinate system $x_{11} - y_{11} - z_{11}$ is fixed in the reference coordinate system $X_0 - Y_0 - Z_0$ and local coordinate system $x_{15} - y_{15} - z_{15}$ is also fixed on the end-effector. Therefore, a transformation matrix E_1 from the end-effector to the coordinate system 5, and S_1 from the coordinate system 1 to frame 0, can be respectively written as

$$E_1 = \begin{bmatrix} 1 & 0 & 0 & 0 \\ 0 & 1 & 0 & 0 \\ 0 & 0 & 1 & f \\ 0 & 0 & 0 & 1 \end{bmatrix}, \quad S_1 = \begin{bmatrix} 0 & 0 & 1 & 0 \\ 1 & 0 & 0 & 0 \\ 0 & 1 & 0 & 0 \\ 0 & 0 & 0 & 1 \end{bmatrix}. \tag{2}$$

Meanwhile, since the direction of the x_{12}-axis is along the common perpendicular direction between z_{11} and z_{12}, and the direction of x_{13}-axis is determined by the vector cross product $z_{12} \times z_{13}$, the following relation holds for the joint angles in the range from $-\pi/2$ to $\pi/2$ associated with the first

https://doi.org/10.1017/S0263574714002732 Published online by Cambridge University Press

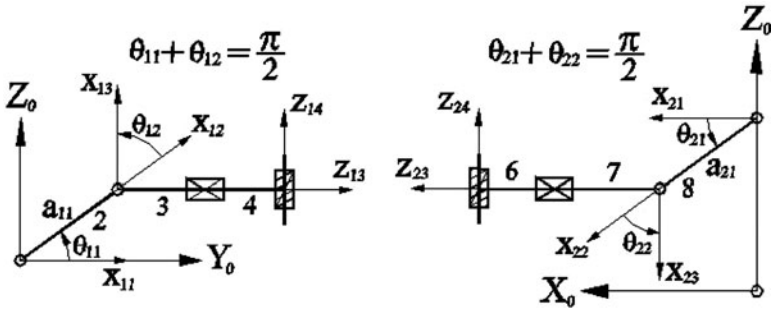

(a) The first limb (b) The second limb

Fig. 3. Geometric relation in joint variables. (a) The first limb, (b) The second limb.

limb as shown in Fig. 3(a).

$$\theta_{11} + \theta_{12} = \frac{\pi}{2}. \tag{3a}$$

A similar relation as shown in Fig. 3(b) can also be obtained for the second limb:

$$\theta_{21} + \theta_{22} = \frac{\pi}{2}. \tag{3b}$$

Thus, the overall D-H transformation matrix from the end-effector to the fixed frame associated with the first limb can be attained by multiplying the above matrices as

$$\begin{aligned} {}^{0}\boldsymbol{T}_{1} &= \boldsymbol{S}_{1}\boldsymbol{A}_{11}\boldsymbol{A}_{12}\boldsymbol{A}_{13}\boldsymbol{A}_{14}\boldsymbol{E}_{1} \\ &= \begin{bmatrix} \cos\theta_{14} & \sin\theta_{14} & 0 & d_{11} \\ \sin\theta_{14} & -\cos\theta_{14} & 0 & a_{11}\cos\theta_{11} + d_{13} \\ 0 & 0 & -1 & a_{11}\sin\theta_{11} - (d_{14} + f) \\ 0 & 0 & 0 & 1 \end{bmatrix}. \end{aligned} \tag{4}$$

Similarly, the coordinate transformation matrices in the second limb can be obtained as

$$\boldsymbol{A}_{21} = \begin{bmatrix} \cos\theta_{21} & -\sin\theta_{21} & 0 & a_{21}\cos\theta_{21} \\ \sin\theta_{21} & \cos\theta_{21} & 0 & a_{21}\sin\theta_{21} \\ 0 & 0 & 1 & -d_{21} \\ 0 & 0 & 0 & 1 \end{bmatrix}, \quad \boldsymbol{A}_{22} = \begin{bmatrix} \cos\theta_{22} & 0 & \sin\theta_{22} & 0 \\ \sin\theta_{22} & 0 & -\cos\theta_{22} & 0 \\ 0 & 1 & 0 & 0 \\ 0 & 0 & 0 & 1 \end{bmatrix},$$

$$\boldsymbol{A}_{23} = \begin{bmatrix} 0 & 0 & -1 & 0 \\ -1 & 0 & 0 & 0 \\ 0 & 1 & 0 & d_{23} \\ 0 & 0 & 0 & 1 \end{bmatrix}, \quad \boldsymbol{A}_{24} = \begin{bmatrix} \cos\theta_{24} & \sin\theta_{24} & 0 & 0 \\ \sin\theta_{24} & -\cos\theta_{24} & 0 & 0 \\ 0 & 0 & -1 & -d_{24} \\ 0 & 0 & 0 & 1 \end{bmatrix}, \tag{5}$$

and

$$\boldsymbol{E}_{2} = \begin{bmatrix} 0 & 1 & 0 & 0 \\ -1 & 0 & 0 & 0 \\ 0 & 0 & 1 & f \\ 0 & 0 & 0 & 1 \end{bmatrix}, \quad \boldsymbol{S}_{2} = \begin{bmatrix} 1 & 0 & 0 & 0 \\ 0 & 0 & 1 & 0 \\ 0 & -1 & 0 & L \\ 0 & 0 & 0 & 1 \end{bmatrix}. \tag{6}$$

https://doi.org/10.1017/S0263574714002732 Published online by Cambridge University Press

The overall D-H transformation matrix from the end-effector to the fixed frame associated with the second limb can be derived as

$$^{0}\boldsymbol{T}_{2}=\boldsymbol{S}_{2}\boldsymbol{A}_{21}\boldsymbol{A}_{22}\boldsymbol{A}_{23}\boldsymbol{A}_{24}\boldsymbol{E}_{2}=\begin{bmatrix}\cos\theta_{24} & \sin\theta_{24} & 0 & a_{21}\cos\theta_{21}+d_{23}\\ \sin\theta_{24} & -\cos\theta_{24} & 0 & d_{21}\\ 0 & 0 & -1 & L-a_{21}\sin\theta_{21}-(d_{24}+f)\\ 0 & 0 & 0 & 1\end{bmatrix}. \tag{7}$$

It can be noted that the third column of both overall transformation matrices are invariant, which indicates the orientation of the end-effector is constant in the direction of z.

3. Kinematic Analysis

3.1. Inverse kinematics

The inverse kinematic analysis of the manipulator provides all possible solutions for the active and passive joint variables when the positions and orientation of the end-effector are given. For the proposed manipulator, the structural parameters L and f, the reduced pitches p_1 and p_2, and the initial values $^{0}d_{14}$ and $^{0}d_{24}$ of two screw pairs and the position (X_E, Y_E, Z_E,) and orientation $\phi(=\theta_{14}=\theta_{24})$ of the end-effector for the CRPH mechanism are given while the translational variables $d_{i1}(i=1,2)$ and rotational variables $\theta_{i1}(i=1,2)$ of the cylindrical pairs, are to be found. Therefore, from Eqs. (4) and (7), equating the elements in the last columns of the posture matrices, three sets of kinematic equations for each limb can be obtained

$$X_E = d_{11} = a_{21}\cos\theta_{21} + d_{23}, \tag{8a}$$

$$Y_E = d_{21} = a_{11}\cos\theta_{11} + d_{13}, \tag{8b}$$

$$Z_E = -(d_{14}+f) + a_{11}\sin\theta_{11} = L-(d_{24}+f) - a_{21}\sin\theta_{21}. \tag{8c}$$

Here, $d_{14} = {}^{0}d_{14} - p_1\theta_{14} = {}^{0}d_{14} - p_1\phi$, and $d_{24} = {}^{0}d_{24} - p_2\theta_{24} = {}^{0}d_{24} - p_2\phi$.

From Eqs. (8a) and (8b), the translational variables of the cylindrical pairs can be directly obtained as $d_{11} = X_E$ and $d_{21} = Y_E$. From Eq. (8c), the rotational variables of cylindrical pairs are solved as follows

$$\theta_{11} = n\pi + (-1)^n \sin^{-1}\left[\frac{Z_E + d_{14} + f}{a_{11}}\right], \tag{9}$$

$$\theta_{21} = n\pi + (-1)^n \sin^{-1}\left[\frac{L - Z_E - d_{24} - f}{a_{21}}\right]. \tag{10}$$

Then, with the geometric relations: $\theta_{11}+\theta_{12}=\pi/2$ and $\theta_{21}+\theta_{22}=\pi/2$, we obtain other passive joint parameters

$$\theta_{12} = \frac{\pi}{2} - \sin^{-1}\left[\frac{Z_E + d_{14} + f}{a_{11}}\right], \tag{11}$$

$$\theta_{22} = \frac{\pi}{2} - \sin^{-1}\left[\frac{L - Z_E - d_{24} - f}{a_{21}}\right]. \tag{12}$$

Finally, from Eqs. (8a) and (8b), the sliding parameters of prismatic joints can be acquired as

$$d_{13} = Y_E - a_{11}\cos\theta_{11}, \tag{13}$$

$$d_{23} = X_E - a_{21}\cos\theta_{21}. \tag{14}$$

https://doi.org/10.1017/S0263574714002732 Published online by Cambridge University Press

3.2. Forward kinematics

In contrast to the inverse kinematics, the forward kinematics solves the positions and the rotation of the end-effector for the CRPH mechanism when the rotary angles $\theta_{i1}(i = 1, 2)$ and the translational displacements d_{i1} $(i = 1, 2)$ of the active cylindrical pairs are given. Based on the equations stated in the previous section, the forward kinematic equations can be solved through both limbs of the manipulator. Positions X_E and Y_E can be obtained directly from Eqs. (8a) and (8b). Moreover, with the relation $\phi = \theta_{14} = \theta_{24}$, Eq. (8c) can be rewritten as

$$Z_E = -{}^0d_{14} + p_1\phi - f + a_{11}\sin\theta_{11}, \tag{15a}$$

$$Z_E = L - {}^0d_{24} + p_2\phi - f - a_{21}\sin\theta_{21}. \tag{15b}$$

To eliminate ϕ in the above equations, we multiply Eq. (15a) by p_2 and Eq. (15b) by p_1, and subtract the two equations. Then, this produces

$$Z_E = \frac{p_2(-{}^0d_{14} - f + a_{11}\sin\theta_{11}) - p_1(L - {}^0d_{24} - f - a_{21}\sin\theta_{21})}{p_2 - p_1}. \tag{16}$$

By substituting Eq. (16) into (15a) yields the rotation angle of ϕ as follows:

$$\phi = \frac{{}^0d_{14} + f - a_{11}\sin\theta_{11}}{p_1} + \frac{p_2(-{}^0d_{14} - f + a_{11}\sin\theta_{11}) - p_1(L - {}^0d_{24} - f - a_{21}\sin\theta_{21})}{p_1(p_2 - p_1)}. \tag{17}$$

The passive joint variables can be obtained via Eqs. (8a) and (8b)

$$d_{23} = X_E - a_{21}\cos\theta_{21}, \tag{18}$$

$$d_{13} = Y_E - a_{11}\cos\theta_{11}. \tag{19}$$

Finally, from Eqs. (3a) and (3b), the passive revolute joint variables is obtained

$$\theta_{12} = \frac{\pi}{2} - \theta_{11}, \tag{20}$$

$$\theta_{22} = \frac{\pi}{2} - \theta_{21}. \tag{21}$$

4. Jacobian and Singularity Analysis

The Jacobian matrix of a parallel manipulator can be derived by differentiating the kinematic constraint equations imposed by the limbs. Let the kinematic equations imposed by the limbs be

$$f(\mathbf{x}, \mathbf{q}) = \mathbf{0}, \tag{22}$$

where $\mathbf{q}$ is a vector containing the actuated joints and $\mathbf{x}$ is the pose vector of the end-effector.

Differentiating the above equation with respect to time, we acquire a relation between the input joint rates and the output velocity of the end-effector[20] as

$$\boldsymbol{J}_x\dot{\boldsymbol{x}} = \boldsymbol{J}_q\dot{\boldsymbol{q}}, \tag{23}$$

where $J_x = \frac{\partial f}{\partial x}$ and $J_q = -\frac{\partial f}{\partial q}$.

Equation (23) leads to two separate Jacobian matrices, the direct Jacobian $\boldsymbol{J}_x$ and the inverse Jacobian $\boldsymbol{J}_q$. A direct kinematic singularity occurs when the determinant of the direct Jacobian $\boldsymbol{J}_x$ is equal to zero, while an inverse kinematic singularity occurs when the determinant of the inverse

https://doi.org/10.1017/S0263574714002732 Published online by Cambridge University Press

Jacobian $\boldsymbol{J}_q$ goes to zero. In what follows, we will investigate the Jacobian and singular conditions of the CRPH manipulator. Differentiating Eqs. (8a), (8b), and (16) with respect to time, we obtain

$$\dot{X}_E = \dot{d}_{11} = -a_{21} \sin\theta_{21}\, \dot{\theta}_{21} + \dot{d}_{23}, \tag{24}$$

$$\dot{Y}_E = \dot{d}_{21} = -a_{11} \sin\theta_{11}\, \dot{\theta}_{11} + \dot{d}_{13}, \tag{25}$$

$$\dot{Z}_E = \frac{(p_2 a_{11} \cos\theta_{11})\, \dot{\theta}_{11} + (p_1 a_{21} \cos\theta_{21})\, \dot{\theta}_{21}}{p_2 - p_1}. \tag{26}$$

Likewise, differentiating Eq. (17) leads to the following result:

$$\dot{\phi} = \frac{(a_{11} \cos\theta_{11})\, \dot{\theta}_{11} + (a_{21} \cos\theta_{21})\, \dot{\theta}_{21}}{p_2 - p_1}. \tag{27}$$

Writing Eqs. (24)–(27) in matrix form derives

$$\begin{bmatrix} \dot{X}_E \\ \dot{Y}_E \\ \dot{Z}_E \\ \dot{\phi} \end{bmatrix} = \begin{bmatrix} 1 & 0 & 0 & 0 \\ 0 & 1 & 0 & 0 \\ 0 & 0 & \frac{p_2 a_{11} \cos\theta_{11}}{p_2 - p_1} & \frac{p_1 a_{21} \cos\theta_{21}}{p_2 - p_1} \\ 0 & 0 & \frac{a_{11} \cos\theta_{11}}{p_2 - p_1} & \frac{a_{21} \cos\theta_{21}}{p_2 - p_1} \end{bmatrix} \begin{bmatrix} \dot{d}_{11} \\ \dot{d}_{21} \\ \dot{\theta}_{11} \\ \dot{\theta}_{21} \end{bmatrix} = J_q \begin{bmatrix} \dot{d}_{11} \\ \dot{d}_{21} \\ \dot{\theta}_{11} \\ \dot{\theta}_{21} \end{bmatrix}. \tag{28}$$

It can be noted that the direct Jacobian $\boldsymbol{J}_x$ is an identity matrix and hence the manipulator has no direct singularity. The singular configurations exist in the inverse kinematic operation of the manipulator. Thus, the zero determinant of the inverse Jacobian matrix $\boldsymbol{J}_q$ in Eq. (28) determines the singular conditions as

$$(p_2 - p_1) \cos\theta_{11} \cos\theta_{21} = 0. \tag{29}$$

Then, we have the following inverse singularity conditions:

$$p_1 = p_2, \tag{30}$$

or

$$\theta_{11} = \frac{(2n-1)\pi}{2} \quad (n = 1, 2, 3, \ldots), \tag{31}$$

or

$$\theta_{21} = \frac{(2n-1)\pi}{2} \quad (n = 1, 2, 3, \ldots). \tag{32}$$

Equation (30) implies that the singularity can be avoided by using distinct values of the pitches of the helical pairs. Eqs. (31) and (32) illustrate two singular conditions for the actuated joint variables, and Fig. 4 shows such a singular configuration. Based on the above analysis, it can be observed that the two rotational input variables play an important role in the singularity analysis of the CRPH robot while the sliding variables have no effect on the singular conditions.

5. Workspace Analysis

The workspace of the robot can be briefly defined as the volume of space that the end-effector can reach. Specifically, it can be further categorized into the reachable and dexterous workspaces,[20,21] where the former means that every point in the volume of the space can be reached in at least one orientation by the end-effector, and the latter indicates every point in the volume of the workspace can be attained in all possible orientations. Thus, the dexterous workspace is a subset of the reachable

https://doi.org/10.1017/S0263574714002732 Published online by Cambridge University Press

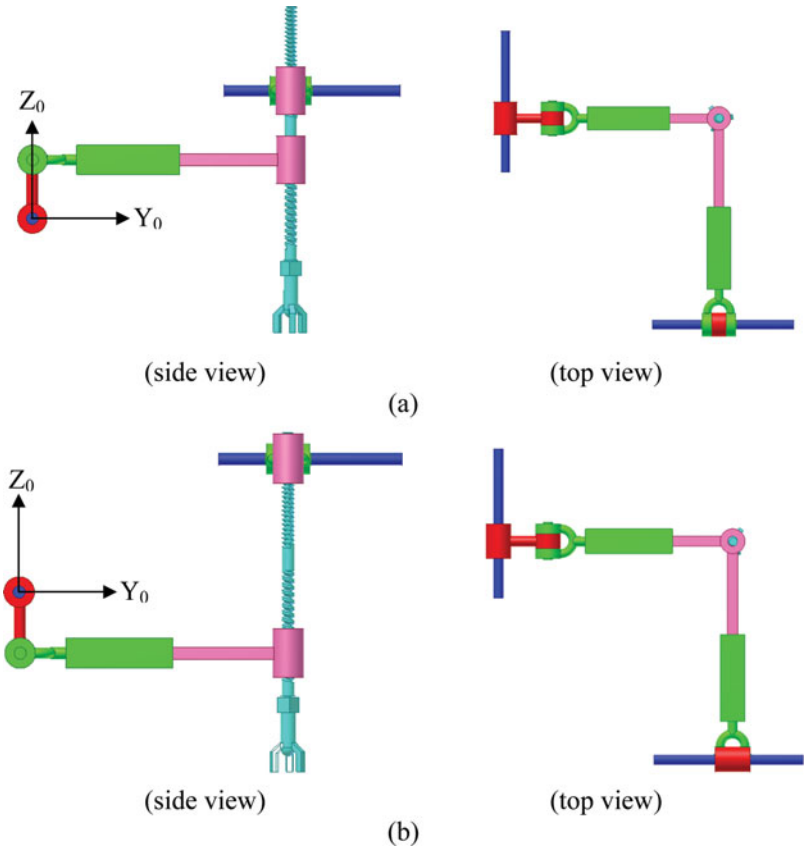

Fig. 4. Two inverse singular configurations.

workspace. Usually, it is not easy to determine the workspace if a parallel manipulator possesses more than three degrees of freedom. However, by varying the design parameters, different types of workspaces can be found. In this paper, the reachable workspace is simulated with respect to different joint parameters for the CRPH manipulator.

In order to view the useful range of the workspace of the CRPH parallel manipulator, the input joint variables are specified as follows:

$$(d_{11})_{\min} \leq d_{11} \leq (d_{11})_{\max}, \tag{33}$$

$$(d_{21})_{\min} \leq d_{21} \leq (d_{21})_{\max}, \tag{34}$$

$$(\theta_{11})_{\min} \leq \theta_{11} \leq (\theta_{11})_{\max}, \tag{35}$$

$$(\theta_{21})_{\min} \leq \theta_{21} \leq (\theta_{21})_{\max}, \tag{36}$$

in which $(d_{i1})_{\min}$ and $(d_{i1})_{\max}$ $(i = 1, 2)$ are the minimal and maximal sliding distances, and $(\theta_{i1})_{\min}$ and $(\theta_{i1})_{\max}(i = 1, 2)$ represent the minimal and maximal rotational angles of the active cylindrical pairs. All the geometric parameters and the boundary values for simulation are assumed and listed in Table II. For the sake of illustration, maximum and minimum limits for the two sliding distances d_{11} and d_{21} are assumed as 50 and 120 cm as shown in Fig. 5. Equations (8a) and (8b) reveal that the reachable workspace projected to X–Y plane is determined by the translational strokes of the actuated cylindrical joints. On the other hand, the volume of the workspace in the z direction is governed by the angles of the active joints since the angles of both actuated joints must be restricted between $+85^\circ$ and -85° to avoid boundary singularities. The ranges of the passive joint variables of the prismatic joints d_{13} and d_{23}, with respect to the active sliding parameters d_{11} and d_{21}, can be obtained as shown in Fig. 6. In fact, these values linearly change with the translational input variables. Figure 7 shows the ranges of the Z_E-position and the orientation ϕ of the end-effector with respect

https://doi.org/10.1017/S0263574714002732 Published online by Cambridge University Press

Table II. Numerical data for workspace simulation..

$a_{11} = a_{21} = 20.0$ cm, $L = 43.5$ cm, $f = 24.0$ cm, ${}^0d_{14} = 24.5$ cm, ${}^0d_{24} = 68.0$ cm, $p_1 = 2.0$ cm, $p_2 = -2.0$ cm, $(d_{11})_{\min} = (d_{21})_{\min} = 50.0$ cm, $(d_{11})_{\max} = (d_{21})_{\max} = 120.0$ cm, $(\theta_{11})_{\min} = (\theta_{21})_{\min} > -85.0^\circ$, $(\theta_{11})_{\max} = (\theta_{21})_{\max} < 85.0^\circ$

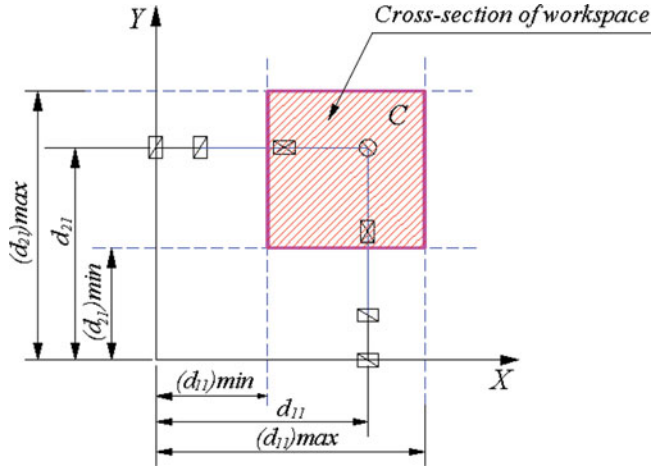

Fig. 5. Workspace in X–Y plane.

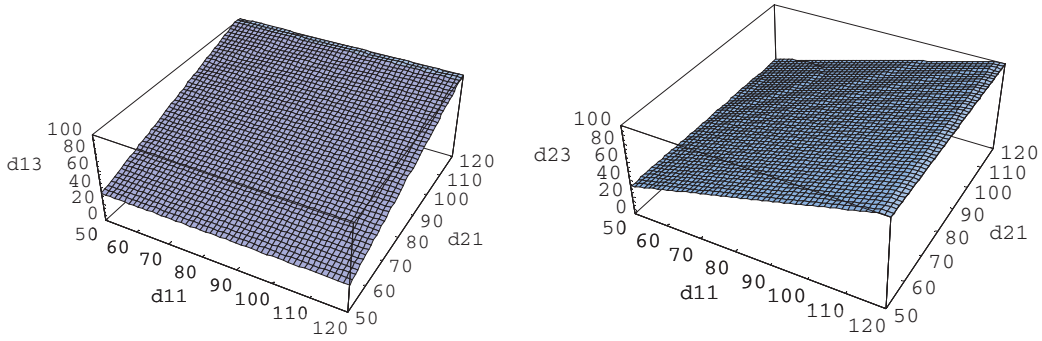

Fig. 6. Passive joints variables vs. d_{11} and d_{21}.

to active joint parameter θ_{11} and θ_{21} while the two translational parameters, d_{11} and d_{21} are fixed. It is worth mentioning that the position along the Z axis of the end-effector is referred to as the Z_E position. It can be noted that the distance between the highest and lowest positions of Z_E is just the architectural lengths of a_{11} and a_{21}. It can be concluded that the shape of the workspace is of a simple rectangular cuboid that does not contain any voids inside the workspace. On the other hand, the workspace formed by the existing robots with Schoenflies motion is usually complex to characterize. For example, the workspace of Delta robots is formed by the intersection of three tori, which usually yields voids inside the workspace and frequently contains workspace-interior singularities.[22]

6. Performance Index

A performance index allows us to quantify the dexterity of a robot. For a serial robot, the manipulability index[23] is commonly used where it measures the volume of the ellipsoid and is developed when mapping from the joint vector space to the end-effector vector space. Another kind of performance index, the condition number, is also widely used where it usually measures the shape condition of the transmission ellipsoid.[24] To measure the performance of the manipulator, the condition number of the Jacobian was used to characterize the serial manipulator by Salisbury and Craig.[25] This condition number can assist designers to judge the isotropy of the manipulators or globally optimize the robot. However, it should be noted that for a manipulator possessing joints of different types, the condition

https://doi.org/10.1017/S0263574714002732 Published online by Cambridge University Press

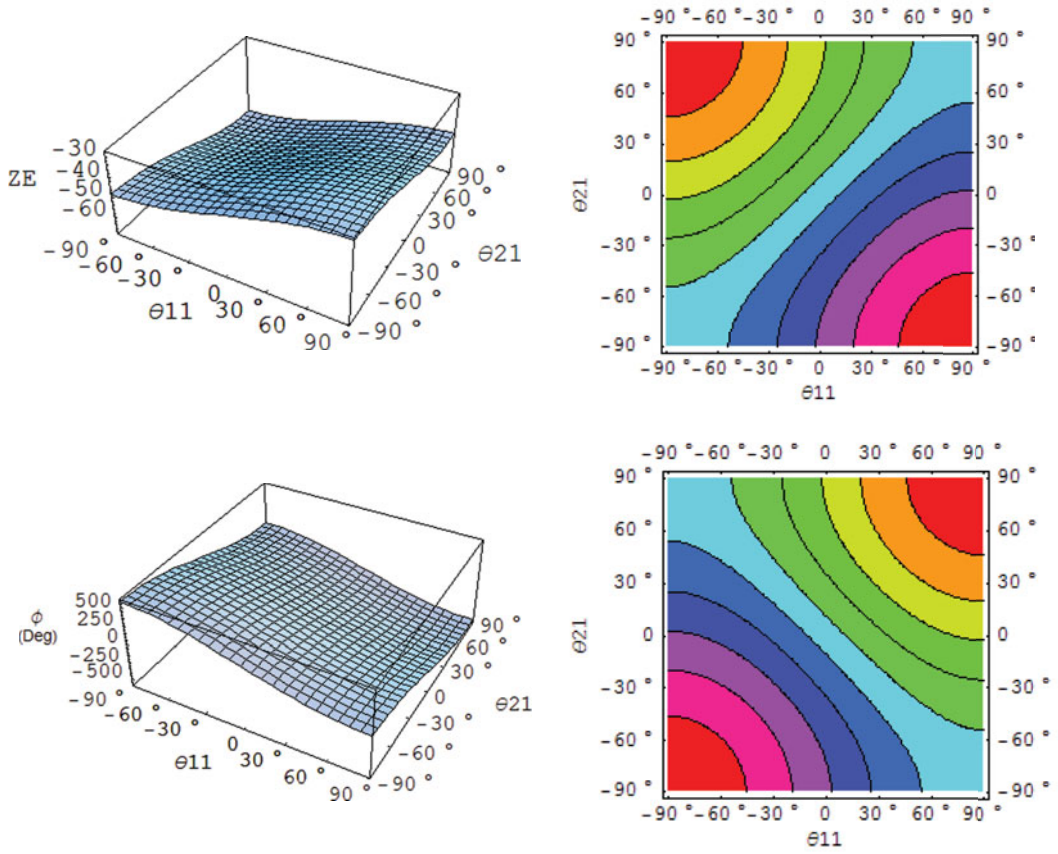

Fig. 7. Surfaces and contours of workspace vs. θ_{11} and θ_{21}.

number of the Jacobian must be carefully dealt with because of the inconsistent dimensions in the elements of the Jacobian matrix.[26] In the paper, the link parameter a_{11} is selected as the characteristic length to unify the dimension of the elements in the Jacobian. That is, some elements that possess length dimension are divided by the characteristic length to become uniform in dimension. In this paper, the condition number of the unified Jacobian based on the Euclidean norm is used to view the performance of the robot since this norm is easier to compute and has a simple explicit expression. The condition number using the Euclidean norm is defined as[24]

$$\kappa(\boldsymbol{J}) = \|J\| \left\|J^{-1}\right\|, \tag{37}$$

with

$$\|J\| = \sqrt{\sum_{i=1}^{i=m} \sum_{j=1}^{j=n} \left|e_{ij}\right|^2},$$

where e_{ij}'s are the elements of the matrix J. Since the condition numbers are configuration dependent, we will show their tendencies by placing the input values of the actuators at some locations rather than demonstrating the numerical results in the whole reachable workspace. Three cases are studied and the characteristics of the results are discussed. In the first case, condition numbers are calculated as the two translational parameters d_{11} and d_{21} of actuators are fixed at a specified value and the angular parameters θ_{11} and θ_{21} vary as shown in Fig. 8. The reciprocal of the condition number is also plotted for the sake of comparison. In the second case, condition numbers are calculated as the two rotational variables θ_{11} and θ_{21} are given a specified value, and d_{11} and d_{21} vary as shown in Fig. 9. Comparing the results of Figs. 8 and 9, it can be seen that the condition numbers are subject

https://doi.org/10.1017/S0263574714002732 Published online by Cambridge University Press

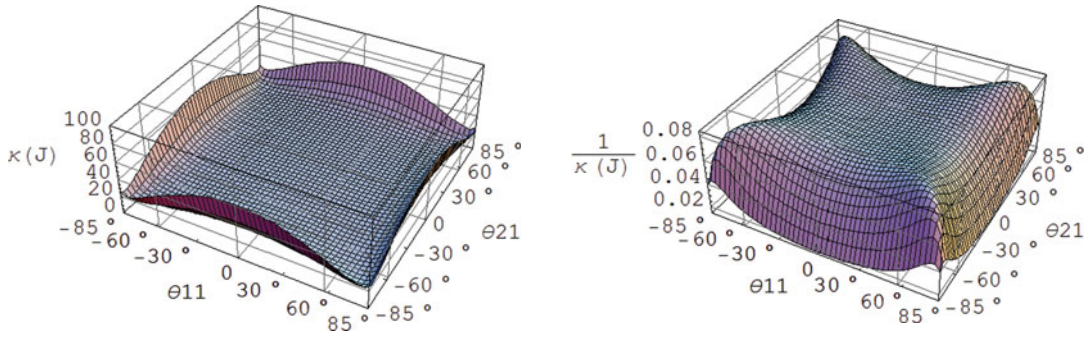

(d_{11}=d_{21}= 94.69cm)

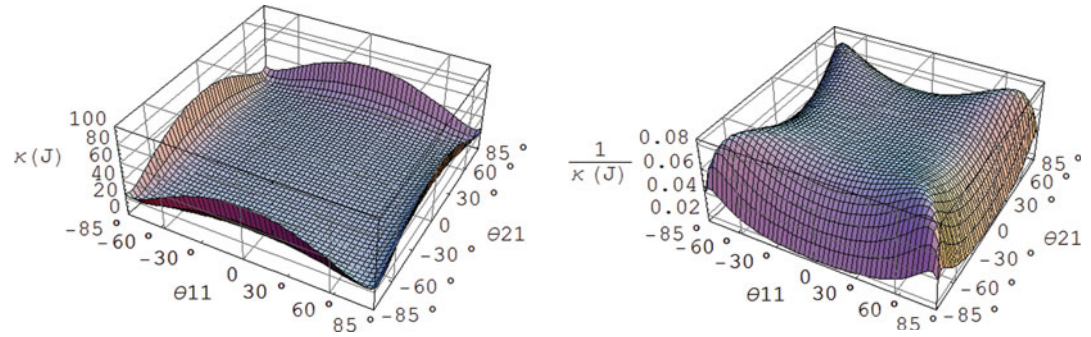

(d_{11}= 100cm, d_{21}= 50cm)

Fig. 8. Condition number and its reciprocal with fixed actuated translations. ($d_{11} = d_{21} = 94.69$ cm); ($d_{11} = 100$ cm, $d_{21} = 50$ cm).

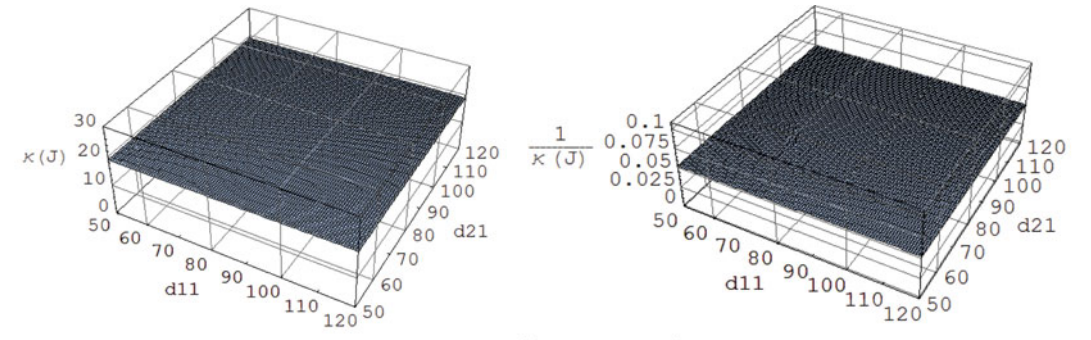

(θ_{11}= −80°, θ_{21}= −60°)

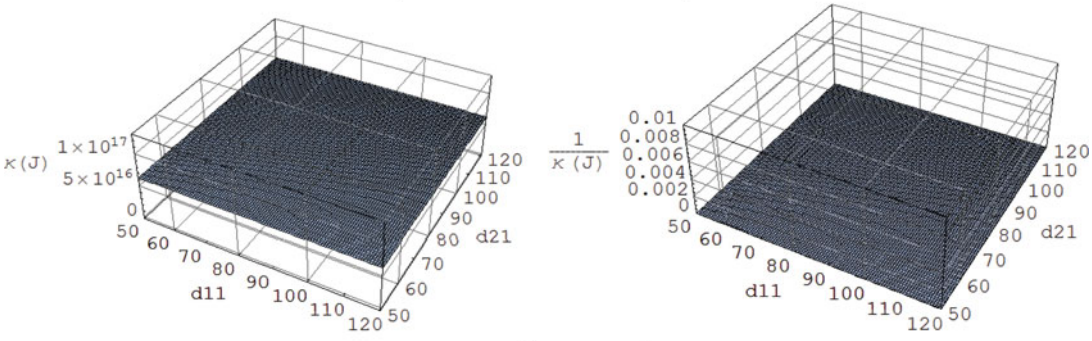

(θ_{11}= 90°, θ_{21}= 45°)

Fig. 9. Condition number and its reciprocal with fixed actuated rotations. ($\theta_{11} = -80°$, $\theta_{21} = -60°$); ($\theta_{11} = 90°$, $\theta_{21} = 45°$).

https://doi.org/10.1017/S0263574714002732 Published online by Cambridge University Press

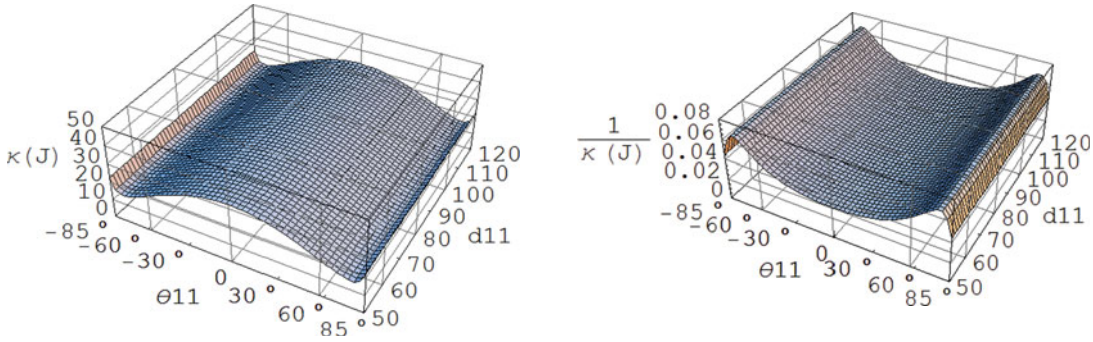

(θ_{21}= -80° , d_{21}= 80cm)

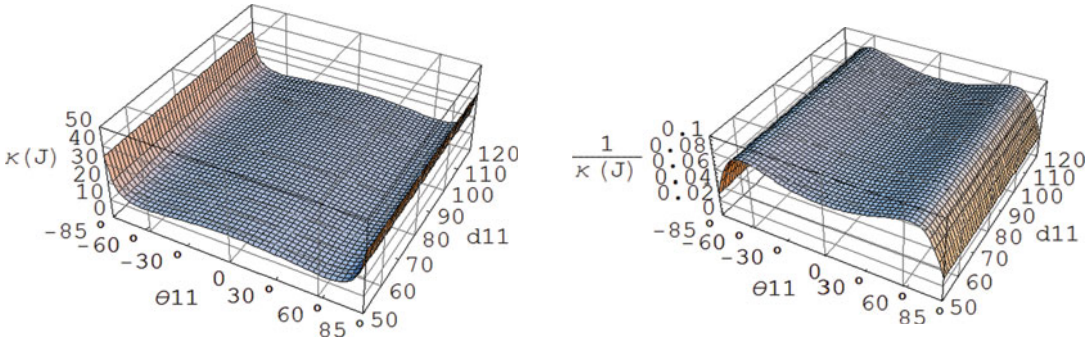

(θ_{21}= -60° , d_{21}= 120cm)

Fig. 10. Condition number and its reciprocal with one fixed limb. ($\theta_{21} = -80^{\circ}, d_{21} = 80$ cm); ($\theta_{21} = -60^{\circ}, d_{21} = 120$ cm).

to the change of two rotational parameters θ_{11} and θ_{21}, yet independent of translational parameters d_{11} and d_{21}. In the second plot of Fig. 9, where the value of θ_{11} is set to 90° on purpose, the condition numbers show the ill conditions of the manipulator regardless of the values of d_{11} and d_{21}. Actually, the singularity of the CRPH manipulator occurs when one of the rotations of the actuators becomes 90 or 270 degrees. In the third case, the condition numbers are calculated as the first limb moves freely while the second limb assumes a specific position as shown in Fig. 10. It can be seen that the singularities occur at $\theta_{11} = +90^{\circ}$ and -90°.

Stan *et al.*[27] have thoroughly studied the performance criteria dealing with workspace, quality transmission, manipulability, and stiffness for the Delta robot with three-DoF translations. They mentioned that all the performance criteria are related to the Jacobian matrix and to the condition number. Compared with the figures for the condition number of the Delta robot shown by Stan *et al.*, the condition number shown by Figs. 8 and 10 appears to be smoother within the working area. In addition, the plots further verify that the ill conditioned workspace is near the boundaries which are in contrast to the existing parallel robots with translational motion whose ill conditions may exist in the workspace.[28] Note that the linear motions of the cylindrical joints have no effect on the condition numbers. This characteristic can also be identified in the Jacobian analysis. Also, only boundary singularities of the manipulator are found within our designated workspace boundary. The manipulator does not contain interior singularities within the workspace.

7. Conclusion

This paper is devoted to investigating the kinematics of one new isoconstrained four-DoF parallel manipulator with Schoenflies motion. The proposed robot has fewer limbs than the general four-DoF fully parallel mechanisms with Schoenflies motion. In addition, the revolution of the end-effector caused by the differential motions of coaxial helical pairs with distinct pitches results in a more

https://doi.org/10.1017/S0263574714002732 Published online by Cambridge University Press

compact structure than the conventional Schoenflies-motion mechanisms. Through the kinematic analysis, it can be seen that the motions of the end-effector activated by the translational actuators and rotational actuators are uncoupled. Thus, it is simple to control the input translation and rotation of the cylindrical pairs to obtain the desired motion of the end-effector. The Jacobian and the singularity analysis also reveal that the singular conditions solely depend on the rotational parameters of the active joints and only boundary singularities are found. The robot is free of interior singularities. This characteristic is also verified by the condition number of the Jacobian. It is expected that this new type of robot has potential applications to industries when it is fully realized.

References

1. D. Stewart, "A platform with 6 degrees of freedom," *Proceedings of Institution of Mechanical Engineers* part 1, **180**(15), 371–386 (1965).
2. R. Clavel, "Delta, A Fast Robot with Parallel Geometry," *18th International Symposium on Industrial Robotics*, Lausanne: IFS Publications (1988) pp. 91–100.
3. R. Clavel, Device for the movement and positioning of an element in space, US Patent 4976582 (1990).
4. J. Angeles, "The qualitative synthesis of parallel manipulators," *ASME J. Mech. Des.* **126**(4), 617–674 (2004).
5. J. Angeles, A. Morozov and O. Navarro, "A Novel Manipulator Architecture for the Production of the SCARA Motions," *Proceedings of IEEE International Conference on Robotics and Automation*, San Francisco, California (2000) pp. 2370–2375.
6. F. Pierrot and O. Company, "H4: A New Family of 4-DoF Parallel Robots," *Proceedings of IEEE/ASME International Conference Advances Intelligent Mechatronics*, Atlanta, GA (1999) pp. 508–513.
7. S. Krut O. Company, M. Benoit, H. Ota and F. Pierrot, "I4: A New Parallel Mechanism for SCARA Motions," *Proceedings of IEEE International Conference on Robotics and Automation*, Taipei, Taiwan (Sep. 14–19, 2003).
8. O. Company and F. Pierrot, "A New 3T-1R Parallel Robot," *Proceedings of the 9th International Conference on Advanced Robotics*, Tokyo, Japan (Oct. 25–27, 1999) pp. 557–562.
9. O. Company, F. Pierrot, V. Nabat and M. Rodriguez, "Schoenflies Motion Generator: A New Non Redundant Parallel Manipulator with Unlimited Rotation Capability," *Proceedings of IEEE International Conference on Robotics and Automation*, Barcelona, Spain (2005) pp. 3250–3255.
10. F. Marquet, O. Company, S. Krut, O. Gascuel and F. Pierrot, "Control of a 3-DoF Over-Actuated Parallel Mechanism," *Proceedings of ASME International Design Engineering Technical Conferences – Computers and Information in Engineering Conference*, Montreal, Canada (2002) DETC2002/MECH-34343.
11. P. L. Richard, C. M. Gosselin and X. W. Kong, "Kinematic analysis and prototyping of a partially decoupled 4-DOF 3T1R parallel manipulator," *ASME J. Mech. Des.* **129**(12), 611–616 (2007).
12. X. W. Kong and C. M. Gosselin, "Type synthesis of 3T1R 4-DoF parallel manipulators based on screw theory," *IEEE Trans. Robot. Autom.* **20**(2), 181–190 (2004).
13. F. Pierrot, V. Nabat, O. Company, S. Krut and P. Poignet "Optimal design of a 4-DOF parallel manipulator: From academia to industry," *IEEE Trans. Robot.* **25**(2), 213–224 (2009).
14. O. Company, S. Krut and F. Pierrot, "Internal singularity analysis of a class of lower mobility parallel manipulators with articulated traveling plate," *IEEE Trans. Robot.* **22**(1), 1–11 (2006).
15. C.-C. Lee and J. M. Hervé, "Isoconstrained parallel generators of Schoenflies motion," *ASME J. Mech. Robot.* **3**(2), 021006 (2011).
16. C.-C. Lee and P.-C. Lee "Isoconstrained Mechanisms for Fast Pick-and-Place Manipulation," *Proceeding of the 1st International Symposium Geometric Methods in Robotics and Mechanism Research*, Hong Kong (Dec. 15–16, 2009).
17. P.-C. Lee, J.-J. Lee and C.-C. Lee, "Four Novel Pick-and-Place Isoconstrained Manipulators and Their Inverse Kinematics," *Proceedings of ASME International Design Engineering Technical Conferences – Computers and Information in Engineering Conference*, Montreal, Quebec, Canada (Aug. 15–18, 2010) DETC2010-28426.
18. P.-C. Lee and J.-J. Lee, "Forward Kinematics and Numerical Verification of Four Novel Parallel Manipulators with Schoenflies motion," *The 1st IFToMM Asian Conference Mechanism and Machine Science*, Taipei, Taiwan (Oct. 21–25, 2010).
19. R. S. Hartenberg and J. Denavit, *Kinematic Synthesis of Linkages* (McGraw-Hill, New York, 1964).
20. L. W. Tsai, *Robot Analysis: The Mechanics of Serial and Parallel Manipulators* (John Wiley & Sons, New York, 1999).
21. J. J. Craig, *Introduction to Robotics: Mechanics and Control*, 3rd ed. (Pearson Prentice Hall, Upper Saddle River, 2005).
22. M. Opl, M. Holub, J. Pavlik, F. Bradac, P. Blecha, J. Kozubik and J. Coufal, "DELTA- Robot with Parallel Kinematics," **In**: *Mechatronics: Recent Technological and Scientific Advances* (Springer, Berlin, 2012) pp. 445–452.
23. T. Yoshikawa, "Manipulability of robotic mechanisms," *Int. J. Robot. Res.* **4**(2), 3–9 (1985).
24. J. P. Merlet, *Parallel Robots*, 2nd ed. (Springer, Dordrecht, 2006).

25. J. K. Salisbury and J. J. Craig, "Articulated hands: Force control and kinematic issues," *Int. J. Robot. Res.* **1**(1), 4–17 (1982).
26. K. E. Zanganeh and J. Angeles, "Kinematic isotropy and the optimum design of parallel manipulators," *Int. J. Robot. Res.* **16**(2), 185–197 (1997).
27. S. Stan, M. Manic, C. Szep and R. Balan, "Performance Analysis of 3 DOF Delta Parallel Robot," *IEEE 4th International Conference on Human System Interactions*, Yokohama, Japan (May 19–21, 2011).
28. R. E. Stamper, L. W. Tsai and G. C. Walsh, "Optimization of a Three DOF Translational Platform for Well-Conditioned Workspace," *Proceedings of IEEE International Conference on Robotics and Automation*, Albuquerque, New Mexico (1997) pp. 3250–3255.

https://doi.org/10.1017/S0263574714002732 Published online by Cambridge University Press